Available online at www.sciencedirect.com
ScienceDirect
Journal of Sound and Vibration 307 (2007) 545–563
JOURNAL OF SOUND AND VIBRATION
www.elsevier.com/locate/jsvi

Discontinuous compliance nonlinearities in the hydraulic engine mount

Song He, Rajendra Singh*

Acoustics and Dynamics Laboratory, Department of Mechanical Engineering, Center for Automotive Research, The Ohio State University, Columbus, OH 43210, USA

Received 14 December 2005; received in revised form 27 December 2006; accepted 13 June 2007
Available online 4 September 2007

Abstract

In this article, we identify and quantify discontinuous compliance nonlinearities of hydraulic engine mounts. First, asymmetric nonlinearities are identified in transient step-up and step-down responses by using a quasi-linear mount model with parameters that are estimated from measured dynamic stiffness data. Second, an improved multistaged top chamber compliance model is developed which confirms the existence of highly nonlinear region(s) during the step transitions as well as during the decaying transients. Third, new semi-analytical solutions for both step-up and step-down responses have been successfully constructed by using a linear time-varying system formulation that incorporates time-varying compliance. Fourth, a mean displacement-dependent model is proposed for the bottom chamber compliance. It clearly explains the stiffening effect in measurements under higher mean loads. Finally, competing quasi-linear, linear time-varying and nonlinear formulations are comparatively evaluated for step and realistic excitations. Transient measurements confirm the validity of models, as well as their applicability and limitations.

1. Introduction

Hydraulic engine mounts are highly nonlinear devices and their cross-point dynamic stiffnesses (K) significantly vary with the amplitude (X) and frequency (f) of sinusoidal excitation [1–4]. Their steady-state characteristics have been extensively reported, usually in the form of $K(f, X)$, based on experimental and analytical studies [1–10]. However, under transient and realistic loading conditions, new nonlinear phenomena emerge. These include asymmetric step responses [11,12] and the stiffening of chambers under increased mean load. Such responses cannot be explained by the existing models [1–14]. Therefore, an in-depth study is needed to investigate the discontinuous nature of the top and bottom chamber compliances. This is the main focus of this article.

The following literature is reviewed with focus on nonlinear top chamber compliance (C_1) and bottom chamber compliance (C_2) models and associated bench tests. Specific mount nonlinearities were first investigated by Kim and Singh [2,3] who measured the nonlinear C_1 and C_2 as well as the inertia track resistance (R_i) of a

*Corresponding author. Tel.: +1 614 292 9044; fax: +1 614 292 3163.
E-mail address: singh.3@osu.edu (R. Singh).

0022-460X/$ - see front matter © 2007 Elsevier Ltd. All rights reserved.
doi:10.1016/j.jsv.2007.06.053

fixed decoupler mount from bench experiments. Colgate and Chang [4] tested several mounts under dual sinusoidal excitations on an elastomer test machine and proposed two separate linear models for large and small amplitudes. Royston and Singh [5] employed Kim and Singh's model [3] as a localized nonlinearity and examined its effect on the vibratory power transmission. Jeong and Singh [6] suggested a nonlinear time-domain model based on a quasi-linear model with frequency- and amplitude-dependent parameters. Further, Geisberger et al. [7] have tested fluid chamber compliances, inertia track and decoupler parameters. Jazar and Golnaraghi [8,9] proposed a simplified nonlinear mathematical model in terms of the Duffing's equation (continuous nonlinearity). Foumani et al. [10] conducted a sensitivity analysis and concluded that C_1 and inertia track inertance I_i are the most influential parameters in the dynamic stiffness over the lower frequency range, while C_1 and decoupler inertia m_d are more influential at higher frequencies. Tiwari et al. [11] refined the bench experiments that were initially proposed by Kim and Singh [3] and further quantified C_1 and C_2 parameters under several preloads. Also, they investigated the vacuum formation that was first observed by Kim and Singh [2,3]. They [12] also examined the mount behaviors to several transient excitations and successfully predicted the transient responses based on a nonlinear formulation with experimentally characterized parameters or functions. Recently, we [13] proposed an efficient procedure that estimates the amplitude-sensitive parameters of a quasi-linear model based on measured $K(f, X)$ data.

Other nonlinear mechanisms, such as the decoupler switching actions and nonlinear fluid resistances, could also be dominant under certain operational conditions. One may also refer to [7,11,12] for testing and modeling procedures; for instance, one could measure nonlinear fluid resistances $R_i(q_i)$ and $R_d(q_d)$, where $q_i(t)$ and $q_d(t)$ are the volumetric flow rates through the inertia track and decoupler, respectively. Lee and Kim [14] have proposed an equivalent viscous damping expression for inertia track based on a nonlinear model. Further discussion of such nonlinear issues is beyond the scope of this article.

2. Problem formulation

2.1. Scope and objectives

Although several nonlinear models have been proposed and validated to some extent, some key questions still remain: Are the nonlinear models based on statically measured parameters [2,11] applicable to real-life excitations or operational conditions? Which nonlinearities would be excited under transient conditions, especially when a rapid change in the loading condition takes place, or when the preload F_m itself may also vary with time? Further, how should we comparatively evaluate the competing linear, quasi-linear and nonlinear formulations? Accordingly, we formulate the following objectives for this article: (1) Propose an improved multistaged $C_1(p_1)$ formulation to capture the asymmetric responses including dynamic stiffening and softening (vacuum) effects, where p_1 is the dynamic top chamber pressure. (2) Develop a new semi-analytical model with time-varying $C_1(t)$ to predict the asymmetric step responses. (3) Propose a refined $C_2(x_m)$ formulation to explain the stiffening effect observed under increased mean loads, where x_m is the mean displacement. (4) Validate proposed nonlinear and semi-analytical linear time-varying formulations by comparing predictions with measurements (and with quasi-linear models) under step and realistic excitations.

2.2. Fluid system formulation with nonlinear parameters

Consider the fluid system of Fig. 1 where control volumes are used to describe a free decoupler-type mount [12]. System parameters include the fluid chamber compliances C_1 and C_2 of the top (#1) and bottom (#2) chambers, stiffness k_r and viscous damping b_r of the rubber element (#r), fluid resistance R_i and inertance I_i of the inertia track (#i), inertance I_d and resistance R_d of the decoupler (#d). A composite displacement excitation $x^t(t)$ is applied under a mean load F_m. Here, we will summarize only those equations that are necessary for further development of the nonlinear and semi-analytical models. Considering only the time-varying components, the "virtual" driving point dynamic force $F(t)$ could be defined as follows, where $x(t)$ is the piston displacement, m_r is the mass of rubber element and A_r is the effective piston area:

$$F(t) = m_r\ddot{x}(t) + b_r\dot{x}(t) + k_r x(t) + A_r p_1(t). \tag{1}$$

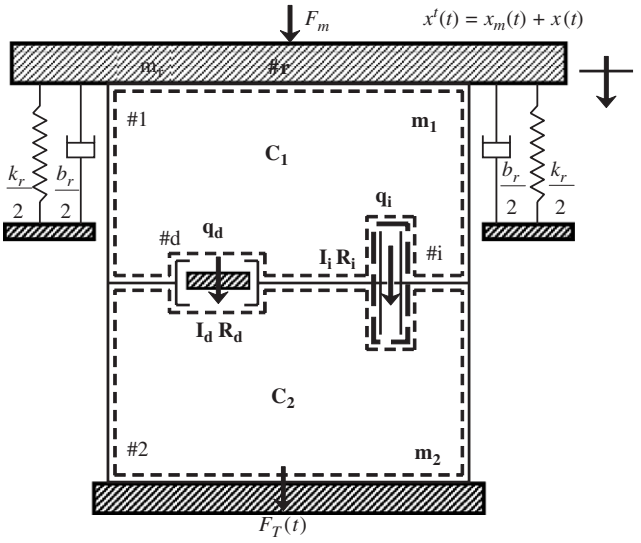

Fig. 1. Lumped fluid model of hydraulic mount with inertia track and decoupler.

Continuity equations for the top and bottom chambers yield the following in terms of nonlinear compliances $C_1(p_1)$ and $C_2(x_m)$ that will be discussed later. Here, $p_2(t)$ is the dynamic pressure in the bottom chamber:

$$A_r\dot{x}(t) - q_i(t) - q_d(t) = C_1(p_1)\dot{p}_1(t), \quad q_i(t) + q_d(t) = C_2(x_m)\dot{p}_2(t). \tag{2,3}$$

Momentum equations for the decoupler and inertia track (with nonlinear resistances) yield the following:

$$p_1(t) - p_2(t) = I_d\dot{q}_d(t) + R_d(q_d)q_d(t), \quad p_1(t) - p_2(t) = I_i\dot{q}_i(t) + R_i(q_i)q_i(t). \tag{4,5}$$

Note that Eq. (4) dictates the "decoupled" state when the decoupler gap is open, and Eq. (5) is dominant over the "coupled" state when the decoupler gap closes. The force transmitted to the rigid base $F_T{}^t(t)$ is often viewed as a measure of mount performance in non-resonant tests [1]. Its dynamic component $F_T(t)$ is related to $F(t)$ as follows:

$$F_T(t) = k_r x(t) + b_r\dot{x}(t) + A_r p_1(t) = F(t) - m_r\ddot{x}(t). \tag{6}$$

3. Discontinuous compliance nonlinearity of top chamber

3.1. Asymmetric step responses

Since $C_2 \gg C_1$ and the fluid springs $k_1 = A_r{}^2/C_1$ and $k_2 = A_r{}^2/C_2$ act in series [13], C_2 dictates the overall fluid path stiffness as well as the mean chamber pressure, while C_1 plays a pivot role in influencing the transient behaviors. Consider transient excitations with a rapid change in the mean load such as the non-ideal step-up and step-down excitations that are shown later in Figs. 6(a) and 7(a). Owing to the limitations of elastomer test machine, smoothened (and not abrupt) transitions with finite slopes exist during the step-up and step-down events. Such excitations could be formulated as $x(t) = X_{\text{amp}}u(t-t_{\text{step}})+X_m$, where t_{step} is the nominal timing of step transition, X_{amp} is the step amplitude, $u(t)$ of unity amplitude denotes either the step-up-like function $u_{\text{up}}(t)$ or the step-down-like function $u_{\text{down}}(t)$, and X_m is the offset in the displacement away from zero before the step event takes place. Significant asymmetries were observed in the measured peak values of $F_T(t)$ and $p_1(t)$ responses [11,12], suggesting a

softening (vacuum) nonlinearity of C_1 during the expansion process, and a dynamic hardening of C_1 during the rapid loading (compressive) event.

3.2. Predictions using a quasi-linear model and comparisons with measurements

In order to quantify the above-mentioned multistaged nonlinearities, experiments were conducted using a take-apart mount (designated as D). Parameters of this mount are as follows: $k_r = 320\text{e}3\,\text{N/m}$, $b_r = 0.5\text{e}3\,\text{N s/m}$, $A_r = 3.31\text{e-}3\,\text{m}^2$, $R_i = 3.45\text{e}7\,\text{kg/s m}^4$, inertia track length $l_i = 0.236\,\text{m}$, $I_i = 2.8\text{le}6\,\text{kg/m}^4$, decoupler damping $b_d = 100\,\text{N s/m}$, decoupler gap length $l_g = 1.1\text{e-}3\,\text{m}$, and $m_d = 6\text{e-}3\,\text{kg}$. The linearized nominal chamber compliances are $C_{10} = 2.5\text{e-}11\,\text{m}^5/\text{N}$ and $C_{20} = 2.4\text{e-}9\,\text{m}^5/\text{N}$. As a first estimate, effective top chamber compliances C_{1e} are approximated by using the quasi-linear model [13] to best curve-fit either the step overshoot or decaying transient given various step excitations. Comparisons of predictions and measurements in Figs. 2–5 show that the quasi-linear model (with a constant C_{1e}) fails to concurrently predict both the overshoot and the decaying transient of step responses due to significant changes in C_{1e} during the step transition.

Compare the estimated C_{1e} values in Table 1(a) with the linearized C_1 values in Table 1(b) that were previously measured [11] at several F_m levels. Note that C_{1e} of the step-up overshoot (from -3.7 to 0 mm) is consistent with the measured C_1 under no preload. Conversely, C_{1e} estimated from the step-down overshoot (from 0 to -3.7 mm) coincides with C_1 measured under $F_m = -1200\,\text{N}$ (or $x_m = -3.7\,\text{mm}$). Meanwhile, C_{1e} values estimated from the decay transients are consistent for all step responses. Also, these C_{1e} values (ranging from 2.17e-11 to 2.99e-11 m^5/N) match well with the nominal C_{10} value (2.5e-11 m^5/N), which is a linearized (and averaged) value based on several operational conditions [11]. The fact that C_{10} lies between the effective C_{1e} values estimated from step-up and step-down overshoots implies that: First, during the unloading (or step-up) process, a dynamic softening effect occurs, which could be explained by the vacuum phenomenon due to a release of dissolved gas under reduced pressure, as suggested by Kim and Singh [2] and Adiguna et al. [12]. Second, a dynamic stiffening effect takes place during the loading (or step-down) process. Third, a linear

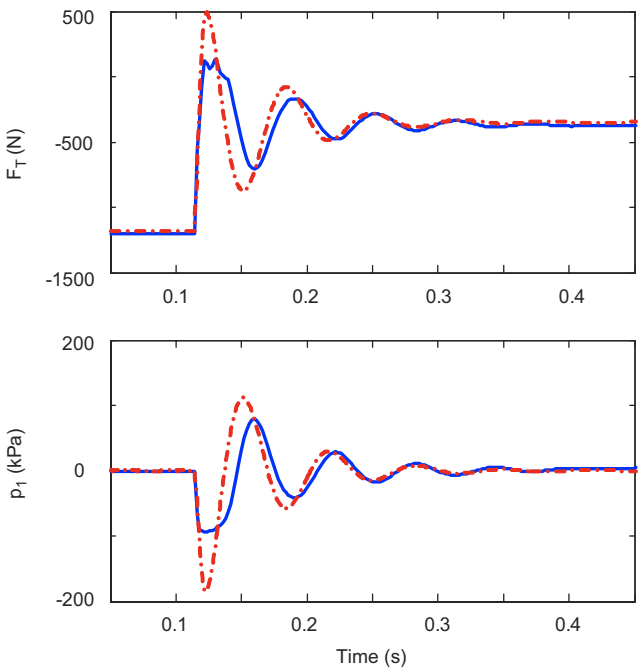

Fig. 2. Transient responses to non-ideal step-up (x_m from -3.7 to -1.32 mm) excitation. Key: ——, measurements; – · – ·, predictions by quasi-linear model with effective C_{1e} (estimated using the decaying transients).

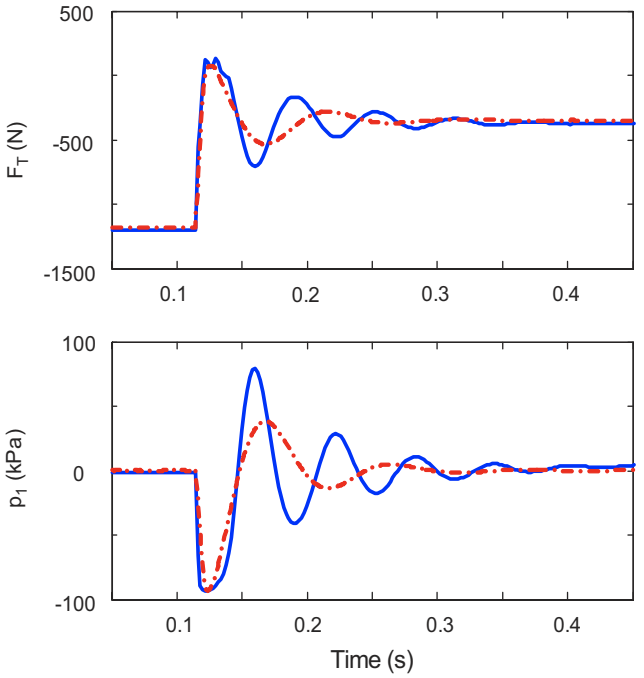

Fig. 3. Transient responses to non-ideal step-up (x_m from -3.7 to -1.32 mm) excitation. Key: ——, measurements; – · – ·, predictions by quasi-linear model with effective C_{1e} (estimated using the overshoot).

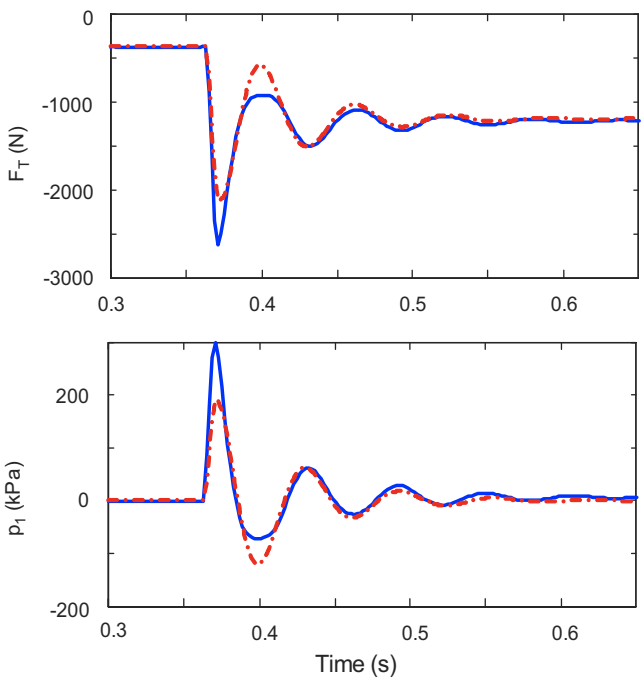

Fig. 4. Transient responses to non-ideal step-down (x_m from -1.32 to -3.7 mm) excitation. Key: ——, measurements; – · – ·, predictions by quasi-linear model with effective C_{1e} (estimated using the decaying transients).

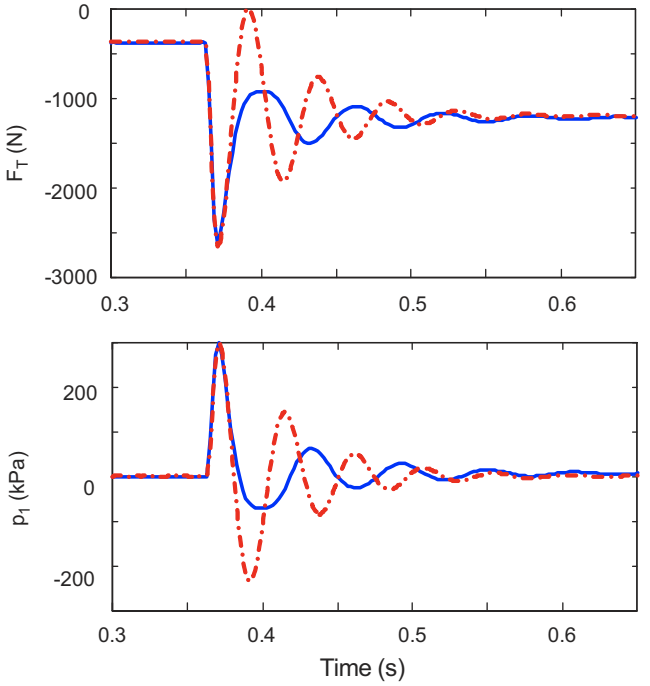

Fig. 5. Transient responses to non-ideal step-down (x_m from −1.32 to −3.7 mm) excitation. Key: ——, measurements; – · – ·, predictions by quasi-linear model with effective C_{1e} (estimated using the overshoot).

Table 1
Estimated or measured top chamber compliance C_1 values

(a) *Effective C_{1e} values estimated from responses to step-up and step-down excitations*		
Non-ideal displacement excitation	C_{1e} (m^5/N) from first overshoot value	C_{1e} (m^5/N) from decaying transient curve
Step-up from −3.7 to 0 mm	7.63e−11	2.99e−11
Step-up from −3.7 to −1.32 mm	5.28e−11	2.45e−11
Step-down from 0 to −3.7 mm	1.09e−11	2.39e−11
Step-down from −1.32 to −3.7 mm	1.26e−11	2.17e−11
(b) *Measured C_1 values from static tests*		
Condition	Static load F_m (N)	Measured C_1 (m^5/N)
Above p_a	0	7.29e−11
	−800	1.05e−11
	−1200	1.09e−11
	−1200	2.5e−11 (C_{10})
Below p_a	$C_1 = -7e{-}45\ p_1^7 + 2.5e{-}11$ (here p_1 is in Pa)	

region exists between the softening and hardening regions, during which a linearized (quasi-linear) model should suffice [13].

3.3. Nonlinear time-varying $C_1(p_1)$ model

Using $p_1(t)$ as a dynamic indicator of operating conditions, the dual-staged $C_1(p_1)$ model [12] is extended to describe the discontinuous nonlinear formulation under vacuum, linear (where C_{10} is the measured compliance

under nominal static load) and dynamic loading conditions as

$$C_1(p_1) = \begin{cases} C_{10} - a_V p_1^{n_V}(t), & p_1(t) < 0 \ \text{(vacuum region)}, \\ C_{10}, & 0 \leqslant p_1(t) \leqslant p_a \ \text{(linear region)}, \\ C_{10} - a_S[p_1(t) - p_a]^{n_S}, & p_a < p_1(t) \ \text{(stiffening region)}. \end{cases} \tag{7}$$

Here, empirical coefficients a_V and a_S as well as polynomial order indices n_V and n_S could be estimated from static measurements [11]. For instance, empirical coefficients for the sample mount (D) are obtained as $a_V = 7\text{e-}45$, $a_S = 1.55\text{e-}33$, $n_V = 7$ and $n_S = 4$. The linearized $C_{10} = 2.5\text{e-}11\,\text{m}^5/\text{N}$ dictates the decaying response, and $p_a = 101$ kPa is the limiting (atmospheric) pressure beyond which significant stiffening effect will occur.

3.4. Predictions by nonlinear model and comparisons with measurements

Considering the complexity introduced by at least two localized nonlinearities such as $C_1(p_1)$ and $C_2(x_m)$, closed-form solutions for $p_1(t)$ or $F_T(t)$ are not feasible. Hence, numerical integration based on the 4/5 order Runge–Kutta algorithm is utilized to simultaneously solve all nonlinear governing equations in time domain. Numerical results should provide insights into interactions between nonlinear elements or processes, which are then expected to lead to semi-analytical treatments. Predicted step-up responses of the fixed decoupler mount using both the multistaged $C_1(p_1)$ and a constant C_{10} are compared with measurements in Fig. 6. Note that the constant C_{10} formulation is clearly not sufficient to capture the vacuum phenomenon featured by the flattened regions in $F_T(t)$ and $p_1(t)$ responses. Predicted time-varying $C_1(t)$ of Fig. 6(d) suggests two response regions including a highly nonlinear initial stage where C_1 is a function of time, and a second decaying stage where C_1 is almost constant (and linear).

Predicted step-down responses of the fixed decoupler mount are compared with measurements in Fig. 7; predictions are again based on the multistaged $C_1(p_1)$ and constant C_{10} models. Dynamic stiffening phenomena are observed during the step-down process, resulting in higher peaks in $F_T(t)$ and $p_1(t)$ responses. Also, the time-varying $C_1(t)$ based on the $C_1(p_1)$ model shows significant and yet smooth reduction during the step-down transition. Although significant vacuum phenomenon is predicted by the nonlinear model, measurements imply that the stiffening effect dominates the transient response. Hence, the step-down response could be approximately predicted (in a piecewise manner) by first employing the time-varying $C_1(t)$ model with hardening characteristics and then utilizing a quasi-linear model with nearly constant C_{10} in the decaying region.

4. Construction of semi-analytical solutions to step responses

4.1. Conceptual time-varying $C_1(t)$ model

A careful comparison between the step-up displacement excitation $x(t)$ of Fig. 6(a) and time-varying $C_1(t)$ of Fig. 6(d) suggests that $C_1(t)$ could be empirically related to the excitation velocity $\dot{x}(t)$. Similar conclusion could also be drawn for step-down responses by comparing $x(t)$ of Fig. 7(a) with $C_1(t)$ of Fig. 7(d) and neglecting the less dominant vacuum effect. Such an interrelationship is conceptually illustrated next.

Assume that gas of mass M and gas constant R is entrained in the top chamber. Also, assume an isothermal process (constant temperature T) during the step transients. Application of the ideal gas law at any instant results in the following equations where $V_{\text{gas}}(t)$ and $p_{\text{gas}}(t)$ are the gas volume and pressure, respectively (with MRT remains constant):

$$p_{\text{gas}}(t) = \frac{MRT}{V_{\text{gas}}(t)}, \quad \text{d}p_{\text{gas}} = -\frac{MRT}{V_{\text{gas}}^2(t)}\,\text{d}V_{\text{gas}}. \tag{8a,b}$$

During the rapid step transition, the fluid exchange between two chambers is negligible due to high inertia track resistance. Thus, we assume a closed system and define an effective (and constant) fluid bulk modulus B_f [15]. Further, assume that only a small amount of entrained gas exists so that the top chamber volume could

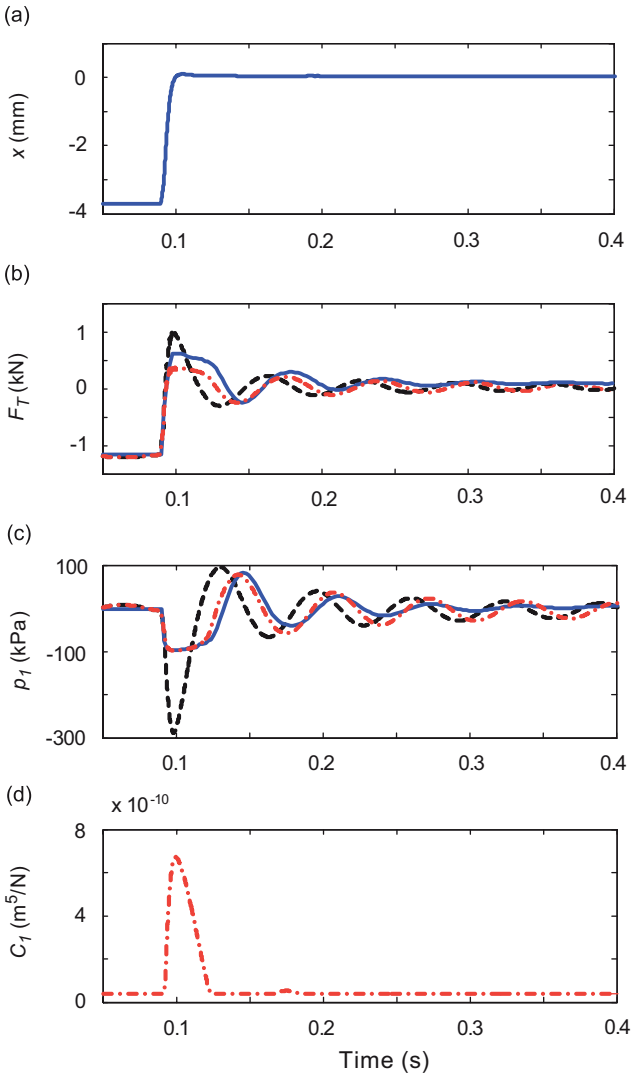

Fig. 6. Step-up responses of a fixed decoupler mount: (a) non-ideal step-up displacement excitation $x(t)$ from -3.7 to 0 mm; (b) transmitted force $F_T(t)$; (c) top chamber pressure $p_1(t)$, and (d) calculated time-varying $C_1(t)$. Key: ——, measurements; – · –, predictions by nonlinear model with multistaged $C_1(p_1)$; – – ·, predictions by nonlinear model with a constant C_{10}.

be approximated by V_{f_0} at the operating point. An infinitesimal change $\mathrm{d}V_f$ is found by applying the Hooke's law as

$$\mathrm{d}V_f = -\frac{V_{f_0}}{B_f}\,\mathrm{d}p_f. \tag{9}$$

The effective $C_{1e}(t)$ could now be derived as follows, where $p_f(t)$ and $p_{\mathrm{gas}}(t)$ correspond to the pressures of fluid and gas components, respectively.

$$C_{1e}(t) = \left|\frac{\mathrm{d}V_{\mathrm{gas}} + \mathrm{d}V_f}{\mathrm{d}p_1}\right| = \frac{(V_{\mathrm{gas}}^2(t)/MRT)\,\mathrm{d}p_{\mathrm{gas}} + (V_{f_0}/B_f)\,\mathrm{d}p_f}{dp_1}. \tag{10a}$$

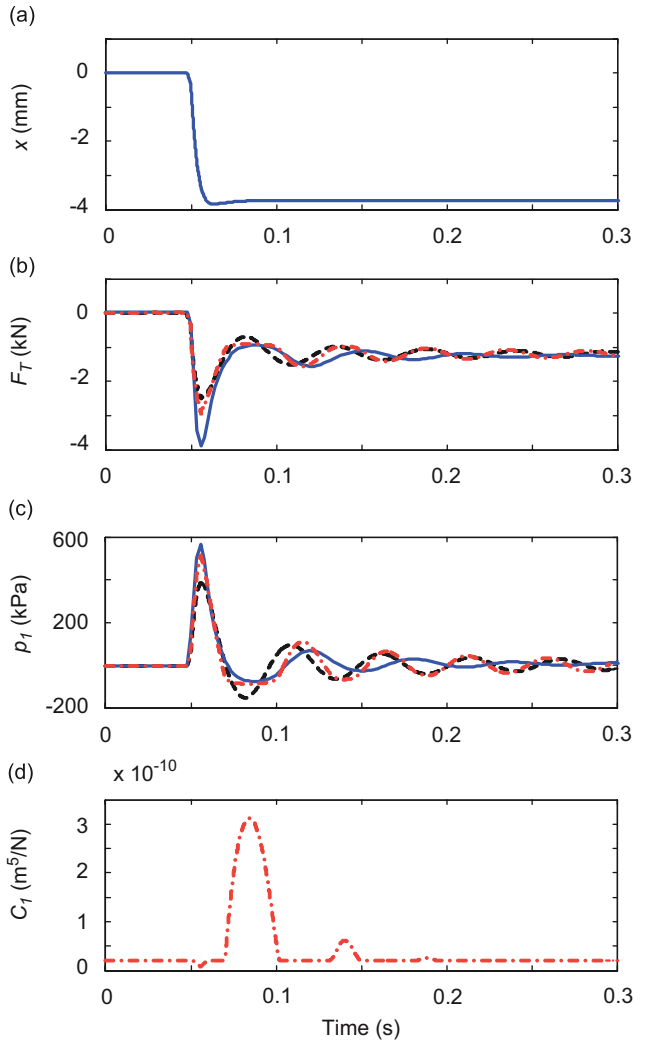

Fig. 7. Step-down responses of a fixed decoupler mount: (a) non-ideal step-down displacement excitation $x(t)$ from 0 to −3.7 mm; (b) transmitted force $F_T(t)$; (c) top chamber pressure $p_1(t)$; and (d) calculated time-varying $C_1(t)$. Key: ——, measurements; – · –, predictions by nonlinear model with multistaged $C_1(p_1)$; – – ·, predictions by nonlinear model with a constant C_{10}.

By assuming $\mathrm{d}p_{\mathrm{gas}} = \mathrm{d}p_f = \mathrm{d}p_1$ during the transient event, we simplify Eq. (10a) as

$$C_{1e}(t) = \frac{V_{\mathrm{gas}}^2(t)}{MRT} + \frac{V_{f_0}}{B_f}. \tag{10b}$$

Linearize the nonlinear $C_{1e}(t)$ formulation at the operating condition (say at $t = t_0$) using the Taylor's-series expansion, and designate $\Delta t = t - t_0$ as the duration of step event:

$$C_{1e}(t) = C_{10} + \frac{\mathrm{d}C_{1e}(t)}{\mathrm{d}t}\Delta t. \tag{11a}$$

Since the bulk modulus of gas alone is much lower than that of the effective fluid bulk modulus ($B_g \ll B_f$), it is assumed that $\mathrm{d}V_{\mathrm{gas}} \gg \mathrm{d}V_f$ so that $\mathrm{d}V_{\mathrm{gas}} \approx A_r\,\mathrm{d}x$. Thus,

$$\frac{\mathrm{d}C_{1e}(t)}{\mathrm{d}t} = \frac{2V_{\mathrm{gas},0}}{MRT}\frac{\mathrm{d}V_{\mathrm{gas}}}{\mathrm{d}t} = \frac{2V_{\mathrm{gas},0}A_r}{MRT}\,\dot{x}(t), \tag{11b}$$

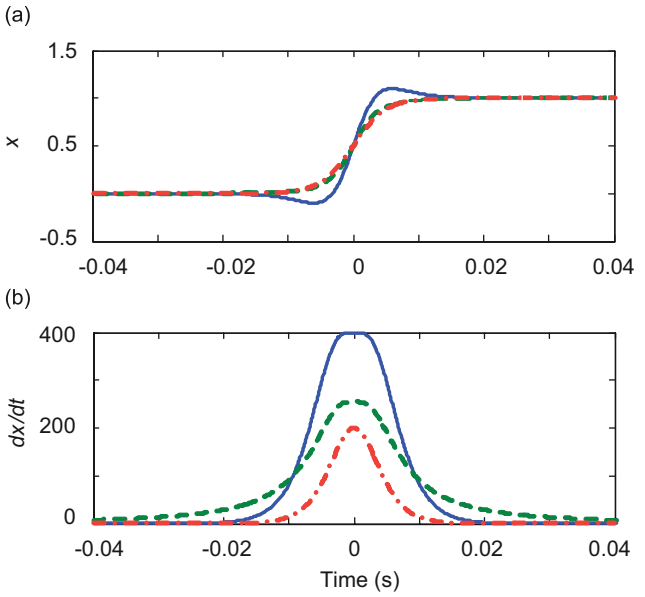

Fig. 8. Comparison of three smoothening functions given $\delta = 100$. Key: ——, hyperbolic-tangent type; – – –, arc-tangent type; – · – ·, hyperbolic-cosine type.

$$C_{1e}(t) = C_{10} + \frac{2V_{\text{gas},0}A_r\Delta t}{MRT}\dot{x}(t). \tag{11c}$$

Here, $V_{\text{gas},0}$ is the gas volume in the top chamber at the operating point. Although the compliance due to rubber element is not considered in our derivation, its contribution is already included in the constant C_{10} (via effective B_f) and thus it should not have much influence on the time-varying component. Further, the time-varying $C_{1e}(t)$ could be related to the excitation velocity, as observed in Figs. 7 and 8. Such an approximation of $C_{1e}(t)$ using $\dot{x}(t)$ would lead to an alternate and yet simplified nonlinear modeling technique as compared to the multistaged $C_1(p_1)$ formulation, since no prior knowledge is needed for the dynamic $p_1(t)$ response. Also, Eq. (11) suggests that the discontinuous nonlinearity of $C_{1e}(t)$ becomes dominant only under significant change in $\dot{x}(t)$. This observation is consistent with earlier findings [13,16] that a quasi-linear model is sufficient to predict responses to simple transients such as the triangular excitations. Despite the assumption that a certain (though small) amount of entrained gas exists in the fluid chamber, additional released gas during the expansion process (depending on the operational conditions) will lead to further softening with an increased value of $C_{1e}(t)$. Likewise, the effect of dissolved gas during the loading procedure will enhance the hardening effect with a lower $C_{1e}(t)$ value. Finally, given all the assumptions and simplifications made in the derivation as well as the difficulty in obtaining an accurate estimate of $V_{\text{gas},0}$ and M, a direct comparison of the analytical prediction based on Eq. (11) with experiments will be difficult. Therefore, Eq. (11) is used as a conceptual model that explains the nonlinear $C_1(t)$ phenomenon though it leads to a semi-analytical study in the next subsection.

4.2. Time-varying C_1 formulation based on smoothening junction approximations

Recall that the experimentally implemented step functions of Figs. 6 and 7 are not ideal transients. Consequently, these excitations could be approximated using the smoothening functions suggested by Kim et al. [17]. This would allow us to develop analytically tractable formulations for step excitations and $C_{1e}(t)$ (based on the implication of Eq. (11)). We approximate the unit step-up excitation $u_{\text{up}}(t)$ by using three types of smoothening functions [17]. Define $\tau = t - t_{\text{step}}$ as the shifted time with respect to the step event; the transition factor δ could be adjusted to tune the slope of smoothened step transition, as a large value of δ

would yield a close approximation of the ideal step function. First, define the unit hyperbolic-tangent-type step-up approximation as

$$u_{\mathrm{up},1}(\tau) = \tanh(\delta\tau) + x[1 - \tanh(\delta\tau)^2]\delta, \tag{12a}$$

$$\dot{u}_{\mathrm{up},1}(\tau) = 2\delta[1 - \tanh(\delta\tau)^2][1 + \tanh(\delta\tau)\delta\tau]. \tag{12b}$$

Second, the unit arc-tangent-type step-up approximation is

$$u_{\mathrm{up},2}(\tau) = \frac{2}{\pi}\arctan(\delta\tau) + \frac{2\delta\tau}{\pi[1 + (\delta\tau)^2]}, \tag{13a}$$

$$\dot{u}_{\mathrm{up},2}(\tau) = \frac{4\delta[1 + 2(\delta\tau)^2]}{\pi[1 + (\delta\tau)^2]^2}. \tag{13b}$$

Third, the unit hyperbolic-cosine-type step-up approximation is

$$u_{\mathrm{up},3}(\tau) = \tanh(\delta\tau), \quad \dot{u}_{\mathrm{up},3}(\tau) = \delta - \tanh(\delta\,\tau)^2\delta. \tag{14a,b}$$

Fig. 8 compares three smoothening functions given $\delta = 100$. Observe that the overall patterns of $u_{\mathrm{up}}(\tau)$ and $\dot{u}_{\mathrm{up}}(\tau)$ resemble those of $x(t)$ and $C_1(t)$ seen earlier in Figs. 6 and 7, although the magnitude of $\dot{u}_{\mathrm{up}}(\tau)$ seems to be higher than that of $C_1(t)$. This suggests that an additional factor is needed to control the peak value of $\dot{u}_{\mathrm{up}}(\tau)$. Likewise, the unit step-down displacement excitations and their derivations are defined as $u_{\mathrm{down},i}(\tau) = -u_{\mathrm{up},i}(\tau)$ and $\dot{u}_{\mathrm{down},i}(\tau) = -\dot{u}_{\mathrm{up},i}(\tau)$, where $i = 1, 2, 3$. The step excitations could be further tuned to achieve realistic magnitudes and yet shifted by a mean component (as seen in realistic vehicle measurements).

Since the time resolution was uniform in experiments, we employ the finite difference method to get an approximation of the first derivative, i.e. $\dot{u}(t) = (\mathrm{d}u/\mathrm{d}t) \approx (\Delta u/\Delta t) = ((u_{i+1} - u_i)/\Delta t)$. Figs. 9 and 10 show that measured step excitations and their first derivatives (though normalized) compare well with the proposed smoothening functions.

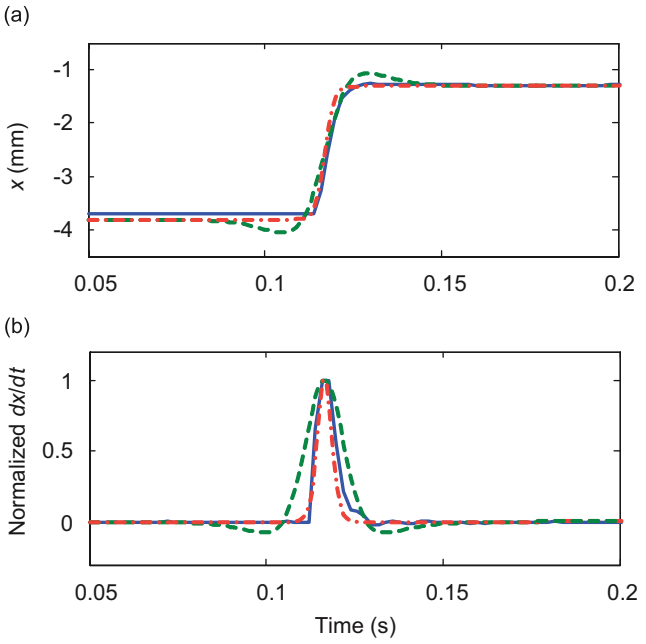

Fig. 9. Comparison of non-ideal step-up excitations and normalized derivatives: (a) $x(t)$; (b) estimation of normalized $\dot{x}(t)$ using finite-difference method. Key: ——, measurement; – –, estimated using hyperbolic-tangent-type function with $\delta = 100$; – · –, estimated using hyperbolic-cosine-type function with $\delta = 400$.

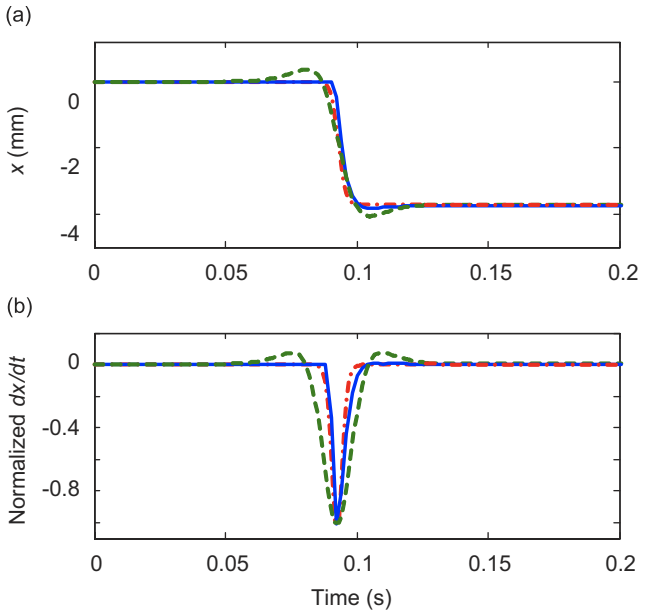

Fig. 10. Comparison of non-ideal step-down excitations and normalized derivatives: (a) $x(t)$; (b) estimation of normalized $\dot{x}(t)$ using finite-difference method. Key: ——, measurement; – – –, estimated using hyperbolic-tangent-type function with $\delta = 100$; – · – ·, estimated using hyperbolic-cosine-type function with $\delta = 400$.

Based on Eq. (11), empirical time-varying $C_1(t)$ expressions are proposed below for step-up excitations using three smoothening functions from Eqs. (12) to (14):

$$C_{1,\mathrm{up},1}(\tau) = 2\delta[1 - \tanh(\delta\tau)^2][1 + \tanh(\delta\tau)\delta\tau]\rho C_{10} + C_{10}, \tag{15}$$

$$C_{1,\mathrm{up},2}(\tau) = \frac{4\delta[1 + 2(\delta\tau)^2]}{\pi[1 + (\delta\tau)^2]^2}\rho C_{10} + C_{10}, \tag{16}$$

$$C_{1,\mathrm{up},3}(\tau) = \delta[1 - \tanh(\delta\tau)^2]\rho C_{10} + C_{10}. \tag{17}$$

Here, C_{10} is the nominal C_1 value corresponding to the linearized operational conditions. In addition to δ, which dictates the shape and slope of the smoothened $x(t)$, we introduce ρ as a tuning factor to control the peak value or the magnitude of $C_1(t)$. Physically, ρ would describe the extent of nonlinearity witnessed during the step transient. Nonlinear predictions based on $C_1(p_1)$ from Figs. 5 and 6 show an increase in the normalized peak value of $C_1(t)/C_{10}$ by up to 6–10 times during the step-up transient, and a reduction in $C_1(t)/C_{10}$ by about 1/3–1/4 during the step-down transient. Meanwhile, typical $\mathrm{d}x/\mathrm{d}t$ values for smoothened functions in Fig. 8 could go up to 400 or even higher. Therefore, a typical ρ value is around 0.01 though it should be empirically tuned. Finally, time-varying $C_1(t)$ expressions are formulated for step-down responses in a similar manner:

$$C_{1,\mathrm{down},1}(\tau) = -2\delta[1 - \tanh(\delta\tau)^2][1 + \tanh(\delta\tau)\delta\tau]\rho C_{10} + C_{10}, \tag{18}$$

$$C_{1,\mathrm{down},2}(\tau) = -\frac{4\delta[1 + 2(\delta\tau)^2]}{\pi[1 + (\delta\tau)^2]^2}\rho C_{10} + C_{10}, \tag{19}$$

$$C_{1,\mathrm{down},3}(\tau) = -\delta[1 - \tanh(\delta\tau)^2]\rho C_{10} + C_{10}. \tag{20}$$

4.3. Step response using a semi-analytical linear time-varying model

Recently we proposed closed-form solutions to ideal step inputs by using a simplified linear (dynamic stiffness type) model [16]. Our analytical predictions correlated reasonably well with measurements except at the first overshoot, where significant asymmetries exist due to the multistaged $C_1(p_1)$ nonlinearity [12,16]. Since $C_1(t)$ is the dominant nonlinearity for step transients, the conceptual model of Eq. (11) provides an efficient way to empirically estimate $C_{1e}(t)$ explicitly from $\dot{x}(t)$ excitations. This also suggests that the $C_{1e}(t)$ expressions of Section 4.2 could be incorporated into a linear model thus leading to a new semi-analytical linear time-varying formulation. Compared with the "true" nonlinear $C_1(p_1)$ model, the semi-analytical solutions could be used to predict only the asymmetric step responses (close to step transitions). Further, such a modeling technique could utilize the effective parameters that are estimated by the quasi-linear model [13] based on measured dynamic stiffness data. Thus, the system identification process should be greatly simplified.

The semi-analytical step-up response of transmitted force is derived as follows:

$$F_{T,\mathrm{up}}(\tau)=\gamma(\tau)\left\{1+\frac{\zeta_1(\tau)}{\sqrt{1-\zeta_2^2(\tau)}}[\mu(\tau)-v(\tau)]e^{-\sigma\tau}\sin[\omega_d(\tau)\tau]+[\mu^2(\tau)-1]e^{-\sigma\tau}\cos[\omega_d(\tau)\tau]\right\}, \tag{21a}$$

where the time-varying mean stiffness function $\gamma(\tau)$ is defined as

$$\gamma(\tau)=k_r+\frac{A_r^2}{C_1(\tau)+C_2}. \tag{21b}$$

And, the expressions for corresponding time-varying natural frequencies $\omega_n(\tau)$ and damping ratios $\zeta(\tau)$ are

$$\omega_{n1}(\tau)=\sqrt{\frac{K_r}{I_i[A_r^2+k_rC_1(\tau)]}},\quad \omega_{n2}(\tau)=\sqrt{\frac{1}{I_iC_1(\tau)}}, \tag{21c,d}$$

$$\zeta_1(\tau)=\frac{1}{2}\sqrt{\frac{R_i^2[A_r^2+C_1(\tau)k_r]}{K_rI_i}},\quad \zeta_2(\tau)=\frac{1}{2}\sqrt{\frac{R_i^2C_1(\tau)}{I_i}}. \tag{21e,f}$$

Further, the two time-varying ratios are defined as

$$\mu(\tau)=\frac{\omega_{n2}(\tau)}{\omega_{n1}(\tau)},\quad v(\tau)=\frac{\zeta_2(\tau)}{\zeta_1(\tau)}. \tag{21g,h}$$

Finally, the damped natural frequency $\omega_d(\tau)$ and decaying exponential index σ are

$$\sigma=\zeta_2(\tau)\omega_{n2}(\tau),\quad \omega_d(\tau)=\omega_{n2}(\tau)\sqrt{1-\zeta_2^2(\tau)}. \tag{21i,j}$$

Note that the index σ, which dictates the exponentially decaying transient, is independent of $C_1(t)$. This explains why the decaying curve predicted using the simplified linear model tends to describe the measured transients reasonably well [16].

Likewise, the step-up response of the dynamic top chamber pressure is derived as

$$p_{1,\mathrm{up}}(\tau)=\lambda\left\{1+\frac{\xi_1[\hat{\mu}(\tau)-\hat{v}(\tau)]}{\sqrt{1-\zeta_2^2(\tau)}}e^{-\sigma\tau}\sin[\omega_d(\tau)\tau]+[\hat{\mu}^2(\tau)-1]e^{-\sigma\tau}\cos[\omega_d(\tau)\tau]\right\}, \tag{23a}$$

where time-invariant static gain λ, natural frequency ϖ_{n1} and damping ratio ξ_1 are

$$\lambda=\frac{A_r}{C_2},\quad \varpi_{n1}=\sqrt{\frac{1}{I_iC_2}},\quad \xi_1=\frac{1}{2}\sqrt{\frac{R_i^2C_2}{I_i}}. \tag{23b–d}$$

Note that the λ expression confirms that the mean chamber pressure is governed by C_2 due to $C_2 \gg C_1$. Here, the two time-varying ratios of parameters are defined as

$$\hat{\mu}(\tau) = \frac{\omega_{n2}(\tau)}{\varpi_{n1}}, \quad \hat{v}(\tau) = \frac{\zeta_2(\tau)}{\xi_1}. \tag{23e,f}$$

Alternately, the $p_{1,\mathrm{up}}(\tau)$ response could also be predicted by using the quasi-linear model [13] as follows, whose parameters could be related to the parameters of an analogous mechanical model [13]; definitions and derivations of top chamber fluid spring k_1, effective inertia track fluid mass m_{ie} and effective inertia track fluid damping b_{ie} are explained in our earlier work [13]:

$$p_{1,\mathrm{up}}(\tau) = \frac{k_1(\tau)}{A_r}\left\{\frac{\zeta_2(\tau)}{\sqrt{1-\zeta_2^2(\tau)}}\sin[\omega_d(\tau)\tau] + \cos[\omega_d(\tau)\tau]\right\}e^{-\sigma\tau}, \tag{24a}$$

$$k_1(\tau) = \frac{A_r^2}{C_1(\tau)} = k_{10}\frac{C_{10}}{C_1(\tau)}, \quad \omega_{n2} = \sqrt{\frac{k_1(\tau)}{m_{\mathrm{ie}}}}, \quad \zeta_2(\tau) = \frac{b_{\mathrm{ie}}}{2\sqrt{k_1(\tau)m_{\mathrm{ie}}}}, \tag{24b–d}$$

$$\sigma = \frac{b_{\mathrm{ie}}}{2m_{\mathrm{ie}}}, \quad \omega_d(\tau) = \omega_{n2}(\tau)\sqrt{1-\zeta_2^2(\tau)}. \tag{24e,f}$$

Similarly, the semi-analytical method could be extended to calculate the step-down responses by using $C_{1,\mathrm{down}}(\tau)$ in place of $C_{1,\mathrm{up}}(\tau)$, and by taking the negative correspondents of step-up responses, i.e. $F_{T,\mathrm{down}}(\tau) = -F_{T,\mathrm{up}}(\tau)$ and $p_{1,\mathrm{down}}(\tau) = -p_{1,\mathrm{up}}(\tau)$.

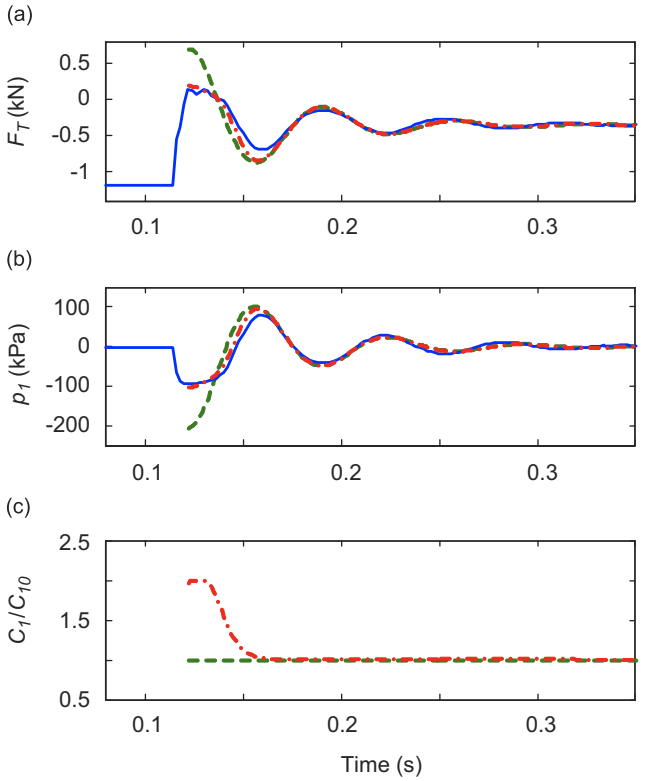

Fig. 11. Comparison of transient responses given non-ideal step-up excitation as shown in Fig. 6(a). Key: ——, measurements; – –, predictions by linear model with constant C_{10}, – · –, predictions by semi-analytical model using hyperbolic-tangent-type smoothening function with $\delta = 100$ and $\rho = 0.005$.

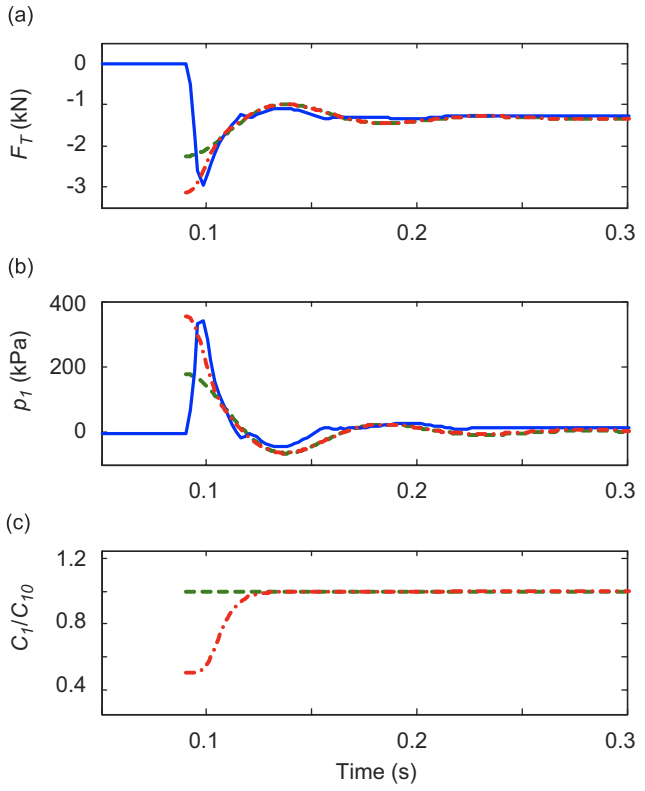

Fig. 12. Comparison of transient responses given non-ideal step-down excitation of Fig. 7(a). Key: ——, measurements; – – –, predictions by linear model with constant C_{10}; – · – ·, predictions by semi-analytical model using hyperbolic-tangent-type smoothening function with $\delta = 100$ and $\rho = 0.005$.

4.4. Comparison of results and validation

The semi-analytical predictions are quantitatively compared with measurements in Figs. 11 and 12 for step-up and step-down responses, respectively. Also, predictions based on the linear time-invariant model with constant C_{10} are displayed. Unlike the "true" nonlinear fluid model described by Eqs. (1)–(7) with multistaged $C_1(p_1)$, our semi-analytical solutions are based on effective parameters that are estimated using the quasi-linear model [13]. Comparisons demonstrate that the semi-analytical model indeed captures both the asymmetric nonlinearities during the step event and the subsequent decaying transients.

5. Discontinuous compliance nonlinearity of bottom chamber

5.1. Features of a realistic displacement profile

Fig. 13 shows a realistic displacement profile, which was measured at the mount location in a front wheel drive vehicle during a typical gearshift event. This transient record contains approximately three seconds of data, and several oscillatory displacements (from 7 to 12 Hz, probably due to wheel hop and/or engine mounting system resonances) are superimposed on the time-varying mean $x_m(t)$ that increases from -4 to -10.5 mm in a piecewise liner manner, corresponding to a shift in the preload F_m from -1200 to -4000 N. The piecewise linear $x_m(t)$ is formulated as

$$x_m(t) = x_{m,j-1} + \frac{x_{m,j} - x_{m,j-1}}{t_j - t_{j-1}}(t - t_{j-1}). \tag{25}$$

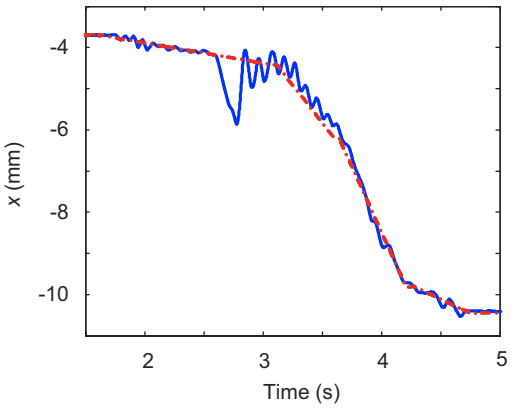

Fig. 13. Realistic displacement excitation measured in a vehicle. Key: ——, composite displacement excitation $x^t(t)$; – · –, time-varying mean displacement $x_m(t)$.

Here, a constant mean displacement slope $\Gamma_i = (x_{m,j} - x_{m,j-1})/(t_j - t_{j-1})$ is assumed within each jth segment. A critical slope $\Gamma_c > \Gamma_i$ could be empirically chosen to distinguish Γ_i from the rapid step excitations. Refer to Fig. 13 for an example case where $\Gamma_c = 3$ mm/s is chosen for the realistic profile. Next, we will focus on the stiffening effect of C_2 induced by $x_m(t)$.

5.2. Stiffening effect of bottom chamber

The bottom chamber is intentionally designed (using thin rubber membrane [11]) to yield a large C_2 to accommodate fluid displaced from the top chamber. Given the complex shape, researchers [1] have assumed a linearized (constant) C_2 value, which is obtained from measurements at a certain operating point. For instance, a nominal value C_{20} of 2.4e-9 m^5/N was measured for mount D and it seems to work well for triangular excitations under a preload F_m of 1200 N. Note that F_m (or x_m) plays a pivot role on the chamber compliances [2,9,10]. First, F_m determines the operating point about which the nonlinear compliances are estimated. Second, F_m dictates the mean fluid pressure (under the static equilibrium) since $C_2 \gg C_1$ and the global compliance of the fluid system is dictated by C_2. For example, the mean pressure measured by Adiguna et al. [12] is virtually equal to the atmospheric pressure when $F_m < 800$ N. However, under real-life operational conditions with a time-varying F_m (or x_m), the bottom chamber membrane expands to accommodate more displaced fluid by the top chamber, and it may gradually loose its property as a very compliant accumulator. Hence, the value of C_2 is reduced under higher F_m (or x_m) and this leads to an increase in the mean chamber pressure, as observed from measurements in Fig. 14. By employing $x_m(t)$ as an indicator of the operational conditions, a piecewise $C_2(x_m)$ model is suggested for the jth segment as follows:

$$C_2(x_m) = C_{2,j-1} + \frac{x_m(t) - x_{m,j-1}}{x_{m,j} - x_{m,j-1}}(C_{2,j} - C_{2,j-1}). \tag{26a}$$

A simplified time-varying $C_2(t)$ is found below by combining Eqs. (25) and (26a), and the incorporation of $C_2(t)$ leads to nonlinear fluid system model:

$$C_2(t) = C_{2,j-1} + \frac{C_{2,j} - C_{2,j-1}}{t_j - t_{j-1}}(t - t_{j-1}). \tag{26b}$$

5.3. Comparison of results and validation

The measured realistic profile of Fig. 13 is implemented in the elastomer test machine as displacement excitations to both fixed and free decoupler hydraulic engine mounts with responses measured in time domain. A comparative study is then conducted using perditions from three competing formulations: (i) quasi-linear

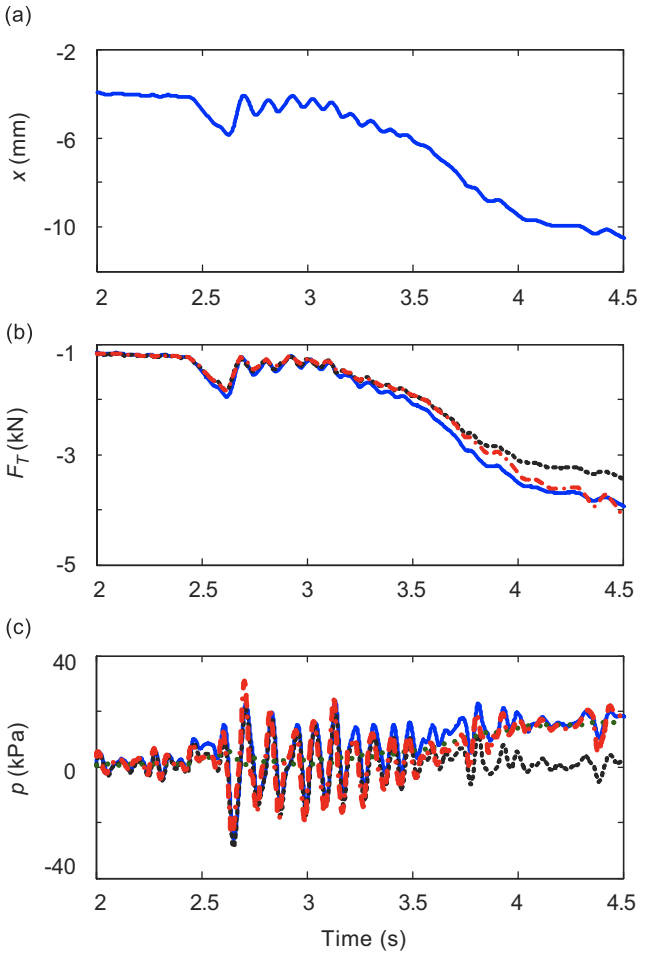

Fig. 14. Transient responses to a realistic profile for a fixed decoupler mount: (a) displacement excitation $x(t)$; (b) transmitted force $F_T(t)$; and (c) chamber pressures $p_1(t)$ and $p_2(t)$. Key: – · –, measurements of $F_T(t)$ or $p_1(t)$; – · –, prediction of $F_T(t)$ or $p(t)$ by quasi-linear model; ——, prediction of $F_T(t)$ or $p_1(t)$ by nonlinear model; ·····, prediction of $p_2(t)$ by nonlinear model with effective $C_{2e} = C_{20}/1.8$.

model [13], (ii) nonlinear fluid model with a constant C_{20}, and (iii) "true" nonlinear $C_2(x_m)$ model. For the fixed decoupler mount, Fig. 14 confirms that the mean pressure built-up effect can only be captured by the $C_2(x_m)$ model though the quasi-linear model is capable of predicting most transient responses. Next, measurements conducted on the free decoupler mount are compared with two nonlinear models (with nominal C_{20} and $C_{2,e}(x_m)$ formulations), as illustrated in Fig. 15; the quasi-linear model is not intentionally chosen since it would not adequately describe the decoupler nonlinearity. Observe that the stiffening effect of C_2 becomes increasingly dominant under higher F_m. Finally, predictions match well with measurements when the effective $C_{2,e}(F_m > 3000\,\text{N}) \approx C_{20}/5$.

6. Conclusion

In this article on discontinuous compliance nonlinearities we have made several contributions to the state of the art in hydraulic engine mounts and related fields. First, asymmetric nonlinearities in responses are identified and clarified under step-up and step-down excitations by using a quasi-linear formulation (with parameters estimated from dynamic stiffness data [13]). An improved multistaged $C_1(p_1)$ model is then developed which confirms the existence of highly nonlinear region(s) during the step transition(s) as well as

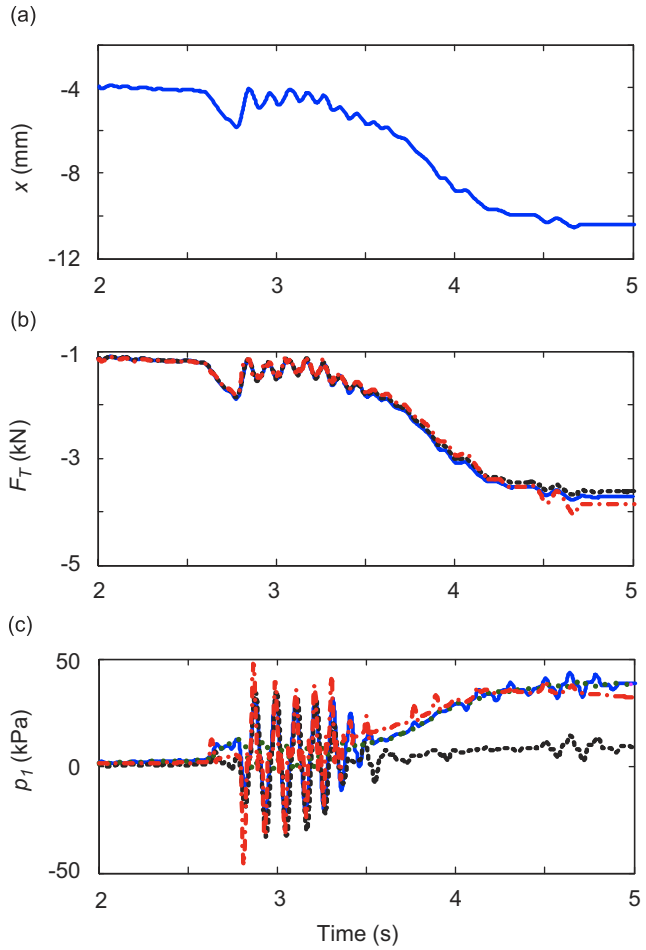

Fig. 15. Transient responses to a realistic profile for a free decoupler mount: (a) displacement excitation $x(t)$; (b) transmitted force $F_T(t)$; and (c) chamber pressures $p_1(t)$ and $p_2(t)$. Key: – · –, measurement of $F_T(t)$ or $p_1(t)$; – – ·, prediction of $F_T(t)$ or $p_1(t)$ by quasi-linear model; ——, prediction of $F_T(t)$ or $p_1(t)$ by nonlinear model; ·····, prediction of $p_2(t)$ by nonlinear model with effective $C_{2e} = C_{20}/5$.

during the decaying transient(s). Further, an analytical model has been developed to conceptually explain a relationship between the effective time-varying $C_{1e}(t)$ and excitation velocity $\dot{x}(t)$. This leads to new approximations of $C_{1e}(t)$ based on alternate smoothening functions. New semi-analytical solutions for step-up and step-down responses have been successfully constructed by using a linear time-varying system formulation that incorporates estimated $C_{1e}(t)$. Further, a mean displacement-dependent compliance $C_2(x_m)$ model for the bottom chamber has been proposed. It clearly explains the stiffening effect in measurements under higher mean loads. Finally, competing quasi-linear, linear time-varying and nonlinear formulations have been comparatively evaluated for step and realistic excitations. Transient measurements confirm the validity of models, as well their applicability and limitations. The benchmark evaluation of this article should aid the analysts in deciding which mount formulation to employ in vehicle models along with efforts that are needed in determining linear and nonlinear parameters as well as errors that might be committed by simplified approaches.

Acknowledgments

We acknowledge the experimental efforts of M. Tiwari and J. Sorenson from 1999 to 2002. Those studies were financially supported by the Ford Motor Company.

References

[1] Y. Yu, N.G. Naganathan, R.V. Dukkipati, A literature review of automotive vehicle engine mounting systems, *Journal of Dynamic Systems, Measurement and Control* 123 (2) (2001) 186–194.

[2] G. Kim, R. Singh, Non-linear analysis of automotive hydraulic engine mount, *Journal of Dynamic Systems, Measurement and Control—Transactions of the ASME* 115 (1993) 482–487.

[3] G. Kim, R. Singh, Study of passive and adaptive hydraulic engine mount systems with emphasis on nonlinear characteristics, *Journal of Sound and Vibration* 179 (3) (1995) 427–453.

[4] J.E. Colgate, C.T. Chang, Y.C. Chiou, W.K. Liu, L.M. Keer, Modeling of a hydraulic engine mount focusing on response to sinusoidal and composite excitations, *Journal of Sound and Vibration* 184 (3) (1995) 503–528.

[5] T.J. Royston, R. Singh, Vibratory power flow through a non-linear path into a multi-resonant receiver, *Journal of Acoustical Society of America* 101 (4) (1997) 2059–2069.

[6] T. Jeong, R. Singh, Inclusion of measured frequency- and amplitude-dependent mount properties in vehicle or machinery models, *Journal of Sound and Vibration* 245 (3) (2001) 385–415.

[7] A. Geisberger, A. Khajepour, F. Golnaraghi, Non-linear modeling of hydraulic mounts: theory and experiment, *Journal of Sound and Vibration* 249 (2) (2002) 371–397.

[8] G.N. Jazar, M.F. Golnaraghi, Non-linear modeling, experimental verification, and theoretical analysis of a hydraulic engine mount, *Journal of Vibration and Control* 8 (1) (2002) 87–116.

[9] M.F. Golnaraghi, N.G. Jazar, Development and analysis of a simplified nonlinear model of a hydraulic engine mount, *Journal of Vibration and Control* 7 (2001) 495–526.

[10] M.S. Foumani, A. Khajepour, M. Durali, Application of sensitivity analysis to the development of high performance adaptive hydraulic engine mounts, *Vehicle System Dynamics* 39 (4) (2003) 257–278.

[11] M. Tiwari, H. Adiguna, R. Singh, Experimental characterization of a nonlinear hydraulic engine mount, *Noise Control Engineering Journal* 51 (1) (2003) 36–49.

[12] H. Adiguna, M. Tiwari, R. Singh, Transient response of a hydraulic engine mount, *Journal of Sound and Vibration* 268 (20) (2003) 217–248.

[13] S. He, R. Singh, Estimation of amplitude and frequency dependent parameters of hydraulic engine mount given limited dynamic stiffness measurements, *Noise Control Engineering Journal* 53 (6) (2005) 271–285.

[14] J.H. Lee, K.J. Kim, An efficient technique for design of hydraulic engine mount via design variable-embedded damping modeling, *Journal of Vibration and Acoustics* 127 (1) (2005) 93–99.

[15] E.O. Doebelin, *System Dynamics: Modeling Analysis, Simulation, Design*, Marcel Dekker, New York, 1998.

[16] S. He, R. Singh, Approximate step response of a non-linear hydraulic mount using a simplified linear model, *Journal of Sound and Vibration* 229 (2007) 656–663.

[17] T.C. Kim, T.E. Rook, R. Singh, Effect of smoothening functions on the frequency response of an oscillator with clearance non-linearity, *Journal of Sound and Vibration* 263 (3) (2003) 665–678.